Seismic vibration mitigation of a multi-story building structure using rate-independent linear damping

Hao Luo[a], Tianyi Zhu[a,*], Zian Tang[a], Shun Weng[a], Hongdi Xiao[a]

[a]*School of Civil and Hydraulic Engineering, Huazhong University of Science and Technology, Wuhan 430074, China*

Abstract

It was well established that rate-independent linear damping (RILD) can benefit base-isolated building structures by reducing the isolator displacement without increasing the floor response acceleration. In the present study, we further extended the application of RILD for seismic vibration mitigation of multi-story building structures. For this purpose, a gradient-based optimization method was presented to determine the locations and required quantities of RILD elements. A ten-story benchmark building structure was employed as an analytical example, and the effectiveness of the proposed method was verified by comparing the performance of the RILD controlled structures using different damper placement methods. Moreover, parametric studies were conducted to investigate the effect of RILD on the dynamic behavior of the optimally controlled structure. The performance curves of the benchmark structure enhanced with optimally placed RILD and viscous dampers were further compared in terms of the control cost and structural inter-story drift. It is suggested that RILD can be advantageous over the conventional viscous damper by more effectively mitigating the seismic vibration response of a multi-story building structure without increasing the control cost.

Keywords: rate-independent linear damping, vibration mitigation, optimal damper placement, multi-story building structure, gradient-based optimization method.

1. Introduction

In the past decades, passive control technologies have been extensively applied for mitigating harmful vibration responses of engineering structures subject to extreme excitations (*i.e.*, strong earthquake and wind) [1, 2]. By installing additional passive energy dissipation systems into engineering structures, the energy dissipation capacity can be increased without requiring a external power source, and the structural vibration amplitude can be reduced. For this purpose, various passive energy dissipation systems have already been developed, *e.g.,* metallic yield dampers [3], friction dampers [4], fluid viscous dampers [5, 6, 7], tuned mass dampers [8, 9], tuned liquid dampers [10, 11], inerter-based dampers [12, 13, 14, 15, 16], negative stiffness dampers [17, 18, 19, 20, 21], and so on.

Different from the viscous damping or nonlinear hysteretic damping in traditional passive energy dissipation systems, rate-independent linear damping (RILD) is an idealized damping model which provides a control force proportional to the deformation whereas in phase with the velocity. It was also known as complex damping, linear hysteretic damping, or structural damping in earlier literatures [22, 23, 24]. Recently, the application of RILD for vibration mitigation of engineering structures have attracted increasing attentions. Inaudi and Kelly [24] obtained the optimal coefficient of RILD for minimizing the mean-square responses of a base-isolation system under stationary random excitations. Ikago and Inoue [25] indicated that RILD is capable of reducing the isolator displacement of a base-isolated structure without increasing floor response accelerations when subjected to strong high-frequency ground motions. Because RILD is non-causal in the time domain [26, 27], many researchers [28, 29, 30, 31, 32, 33, 34] attempted to approximate the behavior of RILD by developing

*Correspondence to: T.Y. Zhu, School of Civil and Hydraulic Engineering, Huazhong University of Science and Technology, Wuhan 430074, China.

Email address: tyzhu@163.com (Tianyi Zhu)

causal models.

More recently, in terms of RILD used for the performance improvement of seismically laoisolated structures, Keivan *et al.* [35, 36] proposed a semi-active method of approximating RILD based on a first-order all-pass filter, and verified its effectiveness by by conducting real-time hybrid simulation tests on seismically isolated structures. Later, in order to passively realize RILD, Luo *et al.* [37] proposed a mechanical model combining a Maxwell element coupled in parallel with a negative stiffness element (hereafter referred to as Maxwell-negative-stiffness (MNS) model). Furthermore, Luo and Ikago [27] proposed a unifying causal model that can include existing causal models of RILD in the literature, and explored its benefits in improving the seismic performance of high-rise building structures. Liu and Ikago [38, 39] implemented the MNS model by using a physical Maxwell-type damper and verified its effectiveness by conducting real-time hybrid simulation tests on a base-isolated structure. Luo *et al.* [40] proposed a novel physical device to realize RILD for performance enhancement of seismically isolated structures. Wu *et al.* [41] presented an inerter-based device to mimic the behavior of RILD for seismic protection of base-isolated structures. Zhu *et al.* [42] examined the feasibility of RILD for simultaneously reducing the isolator and sloshing displacements of base-isolated flexible liquid storage tanks. Luo *et al.* [43] proposed the use of base-isolation systems with RILD for seismic protection of high-rise building structures subject to both near- and far-fault ground motions. It is well established that RILD can benefit a base-isolated structure by effectively reducing the isolator displacement without increasing the structural floor response acceleration, whereas the application of RILD for seismic vibration mitigation of base-fixed building structures is still limited. In the present study, we further explored the benefit of RILD for seismic vibration mitigation of a multi-story shearing building.

To fully utilize the capacities of RILD elements, an optimal design procedure for simultaneously determining their locations and quantities at different stories is to be developed. Indeed, many researchers have worked on the optimal methods of placing damping devices in multi-story shear buildings for seismic performance enhancement. Zhang and Soong [44] presented a sequential procedure for finding the optimal locations of viscoelastic dampers in a frame structure. Later, Wu *et al.* [45] further extended this sequential procedure to 3-D unsymmetrical structures by minimizing translation-torsion coupling effects. Takewaki [46] proposed a gradient-based procedure for optimally placing viscous dampers in a shear building. Later, Takewaki *et al.* [47] further presented a augmented gradient-based procedure for finding the optimal locations and required capacities of added viscous dampers in a 3-D shear building model. Park *et al.* [48] proposed a gradient-based optimization procedure for designing viscoelastic dampers and their supporting braces installed in a structure. Lavan and Levy [49] conducted the fully stressed design method of added viscous dampers installed in a frame structure subject to realistic ground motions. Kanno [50] developed a mixed-integer programming method of optimally placing supplemental viscous dampers used in shear building structures. Martínez *et al.* [51] proposed a optimization procedure for designing nonlinear hysteretic dampers installed in planar structures under seismic excitations. Shen *et al.* [52] presented an elastic–plastic design method of a structure with metallic yield dampers based on the elastic–plastic response reduction curve. Pollini *et al.* [53] pursued the minimum-cost optimization design for seismic retrofitting of structures using nonlinear fluid viscous dampers. Sanati and Karamodin [54] presented an optimum design procedure of frame structures with metallic yielding dampers considering life-cycle cost. Hao *et al.* [55] presented a design method of designing viscoelastic dampers to retrofit reinforced concrete structures based on the structural design capacity redundancy ratio. However, to the best of the authors' knowledge, few research work on the optimization method of designing the locations and required quantities of RILD elements in a multi-story shear building structure have been reported.

In the present study, a gradient-based method was developed to optimally place RILD elements for seismic vibration mitigation of a multi-story shearing building structure, and a ten-story benchmark building structure was employed to verify the effectiveness of the developed method and identify the advantages of RILD over conventional dampers for structural seismic vibration mitigation.

2. Single-degree-of-freedom system

In structural dynamics, damping is an idealized concept to represent a process by which vibra-

tion steadily diminishes in amplitude [56]. Several damping models are available to represent the damping effect for engineering applications, and two types of linear damping model are considered for comparison.

2.1. Two types of linear damping models

2.1.1. Linear viscous damping

The linear viscous damping (LVD) model has been often used to represent damping since its use by Lord Rayleigh [57]. With respect to this model, it is assumed that the resisting force is proportional to relative vocility, *i.e.*,

$$f_1(t) = c_{\mathrm{d}}\dot{x}(t) \tag{1}$$

which f_1 and x are the damping force and relative displacement of the LVD model, respectively; the overdot denotes the derivative with respect to time; c_{d} is the viscous damping coefficient.

By conducting the Fourier transform to Eq.(1), one can reformulate the LVD force in the frequency domain as follows:

$$F_1(i\omega) = i\omega c_{\mathrm{d}} X(i\omega) \tag{2}$$

where i denotes the imaginary unit, and ω is the excitation frequency. From the above equation, the transfer function of an LVD model from the deformation to the resisting force, also known as the dynamic stiffness, is obtained as follows:

$$\mathscr{K}_1(i\omega) = \frac{F_1(i\omega)}{X(i\omega)} = i\omega c_{\mathrm{d}} \tag{3}$$

The LVD model is one of the most widely used linear damping model, which is partly becuase it provides great convenience to the mathematical analyses of structure in both the frequency and time domains. It should be noticed that, in one cycle of harmonic vibration, the energy dissipated by the LVD model can be readily derived as follows:

$$E_1 = \pi\omega c_{\mathrm{d}} X^2 \tag{4}$$

which suggests that the energy dissipated by the LVD model is proportional to the vibration frequency.

2.1.2. Rate-independent linear damping

The RILD model is another type of damping model considered here, and it was first used for the simulation of internal friction in engineering materials. In 1927, Kimball and Lovell [58] reported that, from tests on eighteen solids with different physical properties, the energy loss per sinusoidal strain cycle is proportional to the square of strain amplitude, but independent on the strain rate over a considerable frequency range. This led to the introduction of an idealized concept of RILD.

The resisting force of the RILD model is usually expressed in terms of dynamic stiffness in the frequency domain as follows:

$$\mathscr{K}_2(i\omega) = \frac{F_2(i\omega)}{X(i\omega)} = ik_{\mathrm{d}}\,\mathrm{sgn}\,(\omega) \tag{5}$$

where k_d denote the complex stiffness coefficient; $\mathrm{sgn}(\cdot)$ denotes the signum function. It is suggested that the force of RILD is proportional to the deformation with a phase lead of $\pi/2$ rad. The energy dissipated by the RILD model in one cycle of harmonic vibration is expressed as follows:

$$E_2 = \pi k_{\mathrm{d}} X^2 \tag{6}$$

It is worthy noting that E_2 is independent on the excitation frequency ω. Thus, it can be used to simulate the rate-independent dissipation behavior of some solid materials.

Fig. 1 depicts the dynamic stiffnesses of the LVD and RILD models, where the magnitude of dynamic stiffness is normalized by using the complex stiffness coefficient k_d, and $\omega_0 = k_{\mathrm{d}}/c_{\mathrm{d}}$ denotes a parameter with a unit of circular frequency. It is shown that with $\omega < \omega_0$, RILD generates higher control force compared with LVD. This implies that RILD can more effectively control the structural response displacement under low-frequency excitations. As $\omega > \omega_0$, RILD generates lower control force than LVD. This implies that RILD can avoid generating excessive control force under high-frequency excitations.

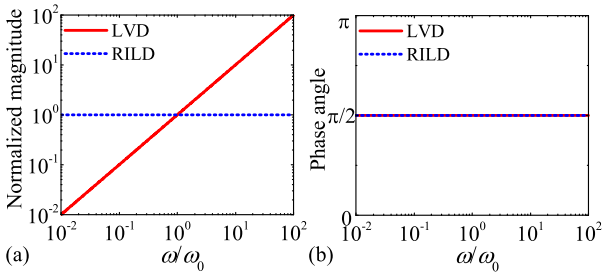

Figure 1: Normalized dynamic stiffness

2.2. Response amplification factors

Let's further consider a generalized linear damping model comprising LVD and RILD elements incorporated into an SDOF structural system, which is governed by the following equation of motion:

$$\left[-m\omega^2 + k + \mathscr{K}_{\mathrm{p}}(i\omega)\right] X(i\omega) = m\omega^2 X_{\mathrm{g}}(i\omega) \quad (7)$$

where m and k denote the structural mass and stiffness, respectively; $X(i\omega)$ and $X_g(i\omega)$ are the frequency-domain response displacement relative to the ground and the excitation acceleration of the ground, respectively; $\mathscr{K}_{\mathrm{p}}(i\omega)$ denotes the dynamic stiffness of the generalized damping model

$$\mathscr{K}_{\mathrm{p}}(i\omega) = i\omega c_{\mathrm{d}} + ik_{\mathrm{d}}\,\mathrm{sgn}\,(\omega) \quad (8)$$

which reduces to Eqs.(3) and (5) in the cases of $k_{\mathrm{d}} = 0$ and $c_{\mathrm{d}} = 0$, respectively. Letting $\omega_1 = \sqrt{k/m}$, $c_{\mathrm{d}} = 2\xi m\omega_1$, $k_{\mathrm{d}} = \eta k$, one can rewrite Eq.(8) as follows:

$$\mathscr{K}_{\mathrm{p}}(i\omega) = im\omega_1\left[2\xi\omega + \eta\omega_1\,\mathrm{sgn}\,(\omega)\right] \quad (9)$$

From Eqs.(7) and (9), one can obtain the relative displacement response amplification factor (RAF) of the damped structural system as follows:

$$D_{\mathrm{RAF}} = \frac{\gamma^2}{\sqrt{(\gamma^2-1)^2 + \left[2\xi\gamma + \eta\,\mathrm{sgn}\,(\gamma)\right]^2}} \quad (10)$$

where $\gamma = \omega/\omega_1$. Similarly, one can also obtain the structural absolute acceleration RAF as follows:

$$A_{\mathrm{RAF}} = \sqrt{\frac{1 + \left[2\xi\gamma + \eta\,\mathrm{sgn}\,(\gamma)\right]^2}{(1-\gamma^2)^2 + \left[2\xi\gamma + \eta\,\mathrm{sgn}\,(\gamma)\right]^2}} \quad (11)$$

For example, letting $\eta = 2\xi$, Fig. 2 depicts the relative displacement and absolute acceleration RAFs of the LVD and RILD damped SDOF structural systems. It is well established that the addition of more LVD can decrease the displacement and acceleration RAFs in the resonant zone at the expense of increased acceleration RAFs at higher frequencies beyond $\omega = \sqrt{2}\omega_0$. However, as shown in Fig. 2, the incorporation of more RILD can achieve a similar reduction in displacement and acceleration RAFs in the resonant zone as LVD, without compromising the high-frequency responses. This indicates that RILD can be more beneficial than LVD in reducing structural response acceleration when it is integrated into base-isolated structures subject to strong earthquake-induced ground motion [18].

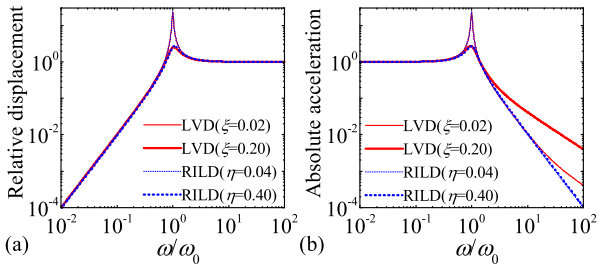

Figure 2: Response amplification factor

It is well established that RILD can effectively reduce the structural response displacement with lower control forces compared with other types of damping devices when subjected to strong ground motions [37]. Several attempts have been made to investigate the effect of RILD on the seismic responses of high-rise building structures [27, 43], however, there is still limited research work on the application of optimally placed RILD elements for the seismic vibration mitigation of building structures.

3. Optimal damping placement

Here, we presented a gradient-based optimization method of placing RILD elements for the seismic vibration mitigation of multi-story building structures.

3.1. Sensitivities of the response amplification factor

Let's consider supplemental generalized linear damping elements incorporated into a multi-degree-of-freedom building structure model, which is governed by the following equation of motion formulated in the frequency domain:

$$\left[-\omega^2\mathbf{M} + i\omega\mathbf{C} + \mathbf{K}_{\mathrm{p}}(i\omega) + \mathbf{K}\right]\mathbf{X}(i\omega) = \omega^2\mathbf{M}\mathbf{1}^T X_g(i\omega) \quad (12)$$

where $\mathbf{M}$, $\mathbf{C}$, and $\mathbf{K}$ are the structural mass, damping, and stiffness matrices, respectively; $\mathbf{X} = \{X_1, X_2, ..., X_n\}^T$ is the displacement vector relative to the ground, where n denotes the story number, and the superscript 'T' denotes the matrix transposition operator; $\mathbf{1} = \{1, 1, ..., 1\}$; $\mathbf{K}_{\mathrm{p}}(i\omega)$ is the dynamic stiffness matrix contributed by supplemental generalized linear damping elements.

By introducing a transformation matrix, *i.e.*,

$$\mathbf{T} = \begin{bmatrix} 1 & 0 & \cdots & 0 & 0 \\ -1 & 1 & \cdots & 0 & 0 \\ \vdots & \vdots & \ddots & \vdots & \vdots \\ 0 & 0 & \cdots & 1 & 0 \\ 0 & 0 & \cdots & -1 & 1 \end{bmatrix} \tag{13}$$

one can formulate the dynamic stiffness matrix of generalized linear damping elements as follows:

$$\mathbf{K}_{\mathrm{p}}(i\omega) = q_{\mathrm{p}}(i\omega)\mathbf{T}^T \mathrm{diag}(\mathbf{k}_{\mathrm{d}})\mathbf{T} \tag{14}$$

where $\mathrm{diag}(\cdot)$ denotes the operation of transforming a vector into the corresponding diagonal matrix; $\mathbf{k}_{\mathrm{d}} = \{k_{d,1}, k_{d,2}, ..., k_{d,n}\}$ denotes a vector of stiffness coefficients of supplemental damping elements; $q_{\mathrm{p}}(i\omega)$ denotes the frequency-dependent term associated with the dynamic stiffness of the p-th type of linear damping element, *i.e.*, one has

$$q_{\mathrm{p}}(i\omega) = \begin{cases} i\omega/\omega_1, & p = 1; \\ i\,\mathrm{sgn}\,(\omega), & p = 2. \end{cases} \tag{15}$$

which are associated with the LVD and RILD elements, respectively.

Furthermore, let's introduce the following auxiliary matrix

$$\mathbf{A} = \frac{1}{\omega_1^2}\left[\mathbf{K} + i\omega_1\mathbf{C} + \mathbf{K}_{\mathrm{p}}(\omega_1) - \omega_1^2\mathbf{M}\right] \tag{16}$$

By substituting Eq.(14) into Eq.(16) and conducting the partial differentiations of the resulting matrix $\mathbf{A}$ with respect to $\mathbf{k}_{\mathrm{d}}$, one can obtain

$$\mathbf{A}'_j = \frac{\partial \mathbf{A}}{\partial k_{d,j}} = \frac{q(i\omega_1)}{\omega_1^2}\mathbf{T}^T\mathbf{D}_j\mathbf{T} \tag{17}$$

with $j = 1, 2, ..., n$, where $\mathbf{D}_j$ denotes a square matrix whose elements are zeros, except for a unity element at the j-th entry in the diagonal.

By using Eq.(16), Eq.(12) can be reformulated as follows:

$$\mathbf{A}\tilde{\mathbf{X}} = \mathbf{M}\mathbf{r}^T \tag{18}$$

with $\tilde{\mathbf{X}} = \mathbf{X}(\omega_1)/X_{\mathrm{g}}(\omega_1)$. By performing partial differentiations of both sides of Eq.(18) with respect to $k_{\mathrm{d},j}$, one has

$$\mathbf{A}'_j\tilde{\mathbf{X}} + \mathbf{A}\tilde{\mathbf{X}}'_j = \mathbf{0} \tag{19}$$

with $j = 1, 2, ..., n$. It follows the first-order sensitivity of the transfer function of relative displacement vector with respect to $k_{\mathrm{d},j}$

$$\tilde{\mathbf{X}}'_j = -\mathbf{A}^{-1}\mathbf{A}'_j\tilde{\mathbf{X}}, \quad j = 1, 2, ..., n. \tag{20}$$

Notice that the inter-story drift vector can be expressed in terms of the relative displacement vector as follows:

$$\hat{\mathbf{U}} = \mathbf{T}\tilde{\mathbf{X}} \tag{21}$$

Similarly, one can obtain the first-order sensitivity of $\hat{\mathbf{U}}$ with respect to $k_{\mathrm{d},j}$ as follows:

$$\hat{\mathbf{U}}'_j = -\mathbf{T}\mathbf{A}^{-1}\mathbf{A}'_j\mathbf{T}^{-1}\hat{\mathbf{U}} \tag{22}$$

Substituting Eq.(17) into Eq.(22) gives

$$\hat{\mathbf{U}}'_j = -\frac{q(i\omega_1)}{\omega_1^2}\mathbf{T}\mathbf{A}^{-1}\mathbf{T}^T\mathbf{D}_j\hat{\mathbf{U}} \tag{23}$$

with $j = 1, 2, ..., n$. Notice that the complex quantity $\hat{\mathbf{U}}$ can also be formulated in terms of its real and imaginary parts as follows:

$$\hat{\mathbf{U}} = \mathrm{Re}[\hat{\mathbf{U}}] + i\ \mathrm{Im}[\hat{\mathbf{U}}] \tag{24}$$

From the above equation, one can obtain

$$\hat{\mathbf{U}}'_j = [\mathrm{Re}(\hat{\mathbf{U}})]'_j + i\ [\mathrm{Im}(\hat{\mathbf{U}})]'_j \tag{25}$$

Therefore, with $\hat{\mathbf{U}}'_j = \{(\hat{U}_1)'_j, (\hat{U}_2)'_j, ..., (\hat{U}_n)'_j\}^T$ obtained from Eq.(23), one can calculate the first-order sensitivity of the RAF of inter-story drift at the l-th story, $|\hat{U}_l|$, with respect to $k_{\mathrm{d},j}$ by using the following equation

$$|\hat{U}_l|'_j = \frac{1}{|\hat{U}_l|}\left(\mathrm{Re}(\hat{U}_l)[\mathrm{Re}(\hat{U}_l)]'_j + \mathrm{Im}(\hat{U}_l)[\mathrm{Im}(\hat{U}_l)]'_j\right) \tag{26}$$

with $l = 1, 2, ..., n$.

Furthermore, by conducting the partial differentiation of Eq.(23) with respect to $k_{\mathrm{d},r}$, one can obtain the following equation

$$\hat{\mathbf{U}}''_{jr} = -\frac{q(i\omega_1)}{\omega_1^2}\mathbf{T}\mathbf{A}^{-1}\left[\mathbf{T}^T\mathbf{D}_j\hat{\mathbf{U}}'_r - \mathbf{A}'_r\mathbf{A}^{-1}\mathbf{T}^T\mathbf{D}_j\hat{\mathbf{U}}\right] \tag{27}$$

where the relation $(\mathbf{A}^{-1})'_r = -\mathbf{A}^{-1}\mathbf{A}'_r\mathbf{A}^{-1}$ is used. On substitution of Eq.(17) into Eq.(27) and use of Eq.(23), the following equation can be obtained

$$\hat{\mathbf{U}}''_{jr} = -\frac{q(i\omega_1)}{\omega_1^2}\mathbf{T}\mathbf{A}^{-1}\mathbf{T}^T\left[\mathbf{D}_j\hat{\mathbf{U}}'_r + \mathbf{D}_r\hat{\mathbf{U}}'_j\right] \tag{28}$$

From the above equation, the real and imaginary parts of $\hat{\mathbf{U}}''_{jr}$ can be obtained, respectively, which are useful to calculate the partial differentiation of Eq.(26) with respect to $k_{\mathrm{d},r}$ as follows:

$$|\hat{U}_l|''_{jr} = \frac{1}{|\hat{U}_l|^2}\{|\hat{U}_l|([\mathrm{Re}(\hat{U}_l)]'_r[\mathrm{Re}(\hat{U}_l)]'_j + \mathrm{Re}(\hat{U}_l)[\mathrm{Re}(\hat{U}_l)]''_{jr} + [\mathrm{Im}$$
$$+ \mathrm{Im}(\hat{U}_l)[\mathrm{Im}(\hat{U}_l)]'_{jr}) - |\hat{U}_l|'_r(\mathrm{Re}(\hat{U}_l)[\mathrm{Re}(\hat{U}_l)]'_j + \mathrm{Im}(\hat{U}_l)[\mathrm{Im}$$

3.2. Formulation of the optimal problem

The objective of the optimal damping placement problem in a multi-story building model is to find optimal $\mathbf{k}_\mathrm{d}$ so that the sum of the structural inter-story drift RAFs at the undamped fundamental frequency is minimized, *i.e.,*

$$\text{Min} \qquad V = \mathbf{1}|\hat{\mathbf{U}}| \tag{30}$$

subjected to constraints on the sums of stiffness coefficients of added linear damping elements

$$\mathbf{1}\mathbf{k}_\mathrm{d} = w \tag{31}$$

where w is a specified constant value. The Lagrangian for the aforementioned problem can be expressed in terms of Lagrange multiplier λ as follows:

$$\mathscr{L}_1(\mathbf{k}_\mathrm{d}, \lambda) = \mathbf{1}|\hat{\mathbf{U}}| + \lambda\left(\mathbf{1}\mathbf{k}_\mathrm{d} - w\right) \tag{32}$$

The optimality criteria for the above problem is obtained from the stationary conditions of $\mathscr{L}(\mathbf{k}_\mathrm{d}, \lambda)$ with respect to $\mathbf{k}_\mathrm{d}$ and λ as follows:

$$\begin{cases} \mathbf{1}|\hat{\mathbf{U}}|'_j + \lambda = 0 \\ \mathbf{1}\mathbf{k}_\mathrm{d} - w = 0 \end{cases} \tag{33}$$

with $j = 1, 2, ..., n$. It is assumed that the stiffness coefficients of added linear damping elements should be non-negative. In the cases of $k_{\mathrm{d},j} = 0$, the corresponding equation of the optimality criteria should be modified as follows:

$$\mathbf{1}|\hat{\mathbf{U}}|'_j + \lambda \geq 0 \tag{34}$$

By introducing the following auxiliary quantities

$$\beta_j = \frac{B_{j+1}}{B_1}, \quad j = 1, 2, ..., n-1. \tag{35}$$

where

$$B_j = \mathbf{1}|\hat{\mathbf{U}}|'_j, \quad j = 1, 2, ..., n. \tag{36}$$

the optimality criteria, Eq.(33), can be alternatively reformulated without the Lagrange multipliers as follows:

$$\begin{cases} \beta_j - 1 = 0 \\ \mathbf{1}\mathbf{k}_\mathrm{d} - w = 0 \end{cases} \tag{37}$$

with $j = 1, 2, ..., n-1$. The linear increment $\Delta\beta_j$ of β_j can be written in terms of increment $\Delta\mathbf{k}_\mathrm{d}$ as follows:

$$\Delta\beta_j = \frac{1}{B_1}\left[(B_{j+1})' - (B_1)'\beta_j\right]\Delta\mathbf{k}_\mathrm{d} \tag{38}$$

where $(B_j)' = \partial B_j/\partial\mathbf{k}_\mathrm{d}$. By combining Eq.(38) with $\mathbf{1}\Delta\mathbf{k}_\mathrm{d} = \mathbf{0}$, one can obtain a set of simultaneous linear equations with respect to $\Delta\mathbf{k}_\mathrm{d}$ as follows:

$$\begin{bmatrix} \frac{1}{B_1}\left[(B_2)' - (B_1)'\beta_1\right] \\ \vdots \\ \frac{1}{B_1}\left[(B_n)' - (B_1)'\beta_{n-1}\right] \\ \mathbf{1} \end{bmatrix}\Delta\mathbf{k}_\mathrm{d} = \begin{Bmatrix} \Delta\beta_1 \\ \vdots \\ \Delta\beta_{n-1} \\ 0 \end{Bmatrix} \tag{39}$$

where the l-th entry in the vector $(B_j)'$ is calculated from the following equation

$$(B_j)'_l = \mathbf{1}|\hat{\mathbf{U}}|''_{jl} \tag{40}$$

with $j, l = 1, 2, ..., n$. Recall that $|\hat{\mathbf{U}}|''_{jl}$ can be obtained from Eq.(29), therefore, one can readily evaluate $\Delta\mathbf{k}_\mathrm{d}$ from Eq.(39) with $\Delta\beta = \{\Delta\beta_1, \Delta\beta_2, ..., \Delta\beta_{n-1}\}^T$ provided. For this purpose, letting

$$\Delta\beta = \frac{1}{N}\left(\beta_\mathrm{F} - \beta_0\right) \tag{41}$$

where β_F and β_0 denote the target and initial values of the quantities defined in Eq.(35), respectively; N denotes the number of incremental steps. From Eq.(37), one can initially assume that $\beta_\mathrm{F} = \{1, 1, ..., 1\}^T$ so that $\Delta\beta$ can be readily evaluated.

It should be mentioned that the stiffness coefficients of supplemental damping elements are non-negative. In the case of $k_{\mathrm{d},j} = 0$, the expression of the optimality criteria in Eq.(37) with respect to β_{j-1} should be modified as follows. For $j = 2, 3, ..., n$, if $k_{\mathrm{d},1} \neq 0$ and $k_{\mathrm{d},j} = 0$, $\beta_{j-1} \leq 1$; if $k_{\mathrm{d},1} = 0$ and $k_{\mathrm{d},j} \neq 0$, $\beta_{j-1} \geq 1$. It should be noticed that a similar formulation was presented by Takewaki [46] to optimally place viscous dampers in shear buildings.

4. Numerical examples

In order to verify the effectiveness of the aforementioned method and illustrate the benefit of RILD, a ten-story benchmark shear building structure [59] was used as an analytical example, as shown in Fig. 3, whose structural parameters are listed in Table 1. Modal analyses were conducted for the undamped primary linear structure, and the first three undamped fundamental natural periods are 2.01 s, 0.76 s, and 0.46 s. The inherent damping matrix of the primary building structure was assumed to be proportional to the structural stiffness matrix with a inherent damping ratio of $\xi_0 = 0.02$, *i.e.*, $\mathbf{C}_0 = 2\xi_0/\omega_1\mathbf{K}$.

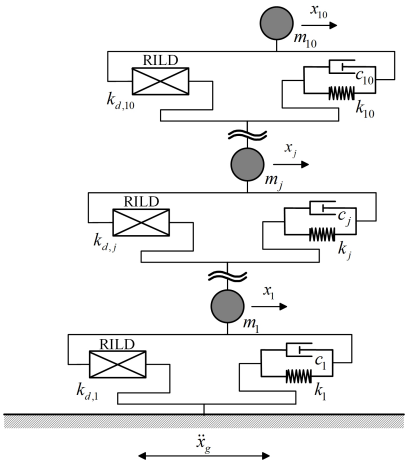

Figure 3: A 10-story benchmark shear building structure

Table 1: Primary structural properties

j	m_j (ton)	k_j (kN/m)	c_j (kN·s/m)	Height (m)
1	700	279 960	3 586	6
2	682	383 550	4 913	4
3	680	383 020	4 906	4
4	676	328 260	4 204	4
5	670	306 160	3 921	4
6	667	291 890	3 739	4
7	660	244 790	3 135	4
8	656	220 250	2 821	4
9	649	180 110	2 307	4
10	875	158 550	2 031	4

4.1. Effectiveness of the optimal method

Additional RILD elements are supplemented to mitigate the vibration of the primary structure under strong earthquakes. For comparison, three different cases are considered: (i) the complex stiffness coefficients of RILD elements are proportional to the structural stiffness coefficients, *i.e.*, ${}_{\mathrm{P}}\mathbf{k}_{\mathrm{d}} = \eta\mathbf{k}$ (proportional case, $\eta = 2\xi = 0.1$ is considered in this example); (ii) the coefficients of RILD elements are uniformly distributed at each story of the building structure (uniform case); (iii) the coefficients of RILD elements are optimally obtained by using the developed method (optimal case, β_0 is obtained from the uniform case). The sums of the complex stiffness coefficients of RILD elements used in the three cases are assumed to be equal. For the last case, $N = 100$ was used in this example. The complex stiffness coefficients of RILD elements obtained in the three cases are also listed in Table 2.

4.1.1. Frequency response analyses

Fig. 4 depicts the inter-story drift and absolute acceleration RAFs of the uncontrolled structure and those of the controlled structure equipped with RILD elements evaluated at the undamped fundamental frequency. It is noticed that in the optimal case, RILD elements are placed in the first and fourth stories (as shown in Table 2), where the inter-story drifts of the uncontrolled structure are larger than those of other stories (see the solid black line in Fig. 4(a)). From Fig. 4, it is observed that compared with the proportional and uniform cases, the structure equipped with optimally placed RILD elements are more effective in reducing both inter-story drift and absolute acceleration RAFs evaluated at the undamped fundamental frequency.

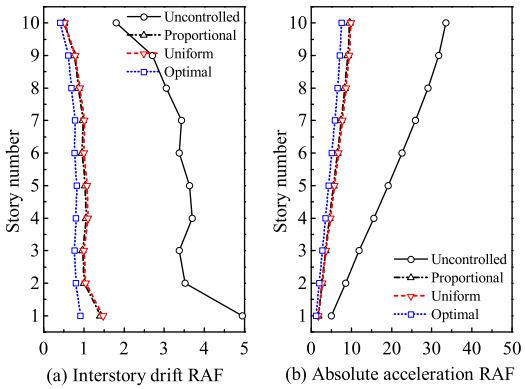

Figure 4: Structural RAFs at the fundamental frequency

Figs. 5 and 6 depict the first story drift and rooftop acceleration RAFs of the controlled structure equipped with RILD elements, respectively. It is shown that compared with other two cases, the optimally placed RILD elements are more effective in reducing the the first story drift RAFs all over the frequency, without compromising the rooftop acceleration RAFs. It is expected that RILD can be used to simultaneous mitigating the response displacement and acceleration of a multi-story building structure subject to strong earthquakes.

4.1.2. Response history analyses

Time-history response analyses were conducted to investigate the performance of the differently controlled benchmark structures under strong earthquakes. For example, Figs. 7 and 8 depict the peak responses of the uncontrolled and controlled

Table 2: Properties of RILD elements in three different cases

j	${}_jk_d$ (kN/m)			β_j		
	Proportional	Uniform	Optimal	Proportional	Uniform	Optimal
1	27 996	27 765	186 748	0.51	0.51	0.88
2	38 355	27 765	0	0.46	0.47	0.82
3	38 302	27 765	0	0.56	0.56	1.00
4	32 826	27 765	90 906	0.54	0.54	0.95
5	30 616	27 765	0	0.47	0.46	0.83
6	29 189	27 765	0	0.48	0.48	0.86
7	24 479	27 765	0	0.38	0.38	0.68
8	22 025	27 765	0	0.30	0.29	0.54
9	18 011	27 765	0	0.14	0.13	0.24
10	15 855	27 765	0	–	–	–

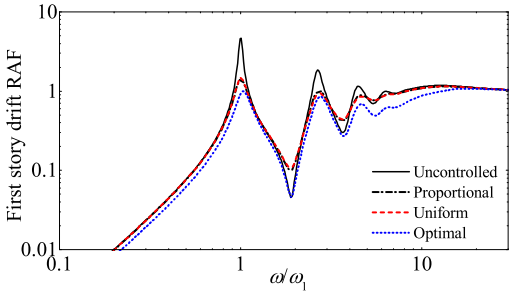

Figure 5: Structural first story drift RAFs

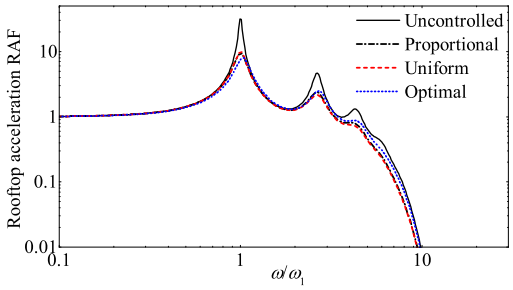

Figure 6: Rooftop absolute acceleration RAFs

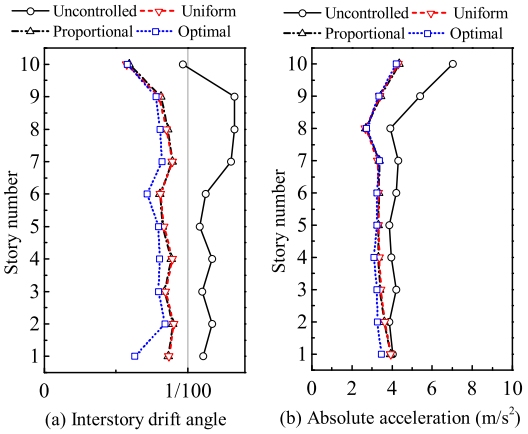

Figure 7: Structural peak floor responses (El Centro)

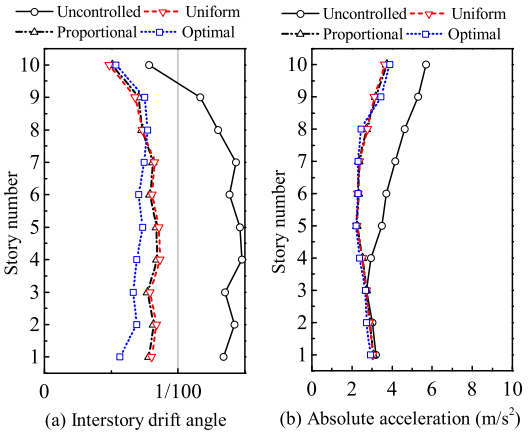

Figure 8: Structural peak floor responses (Hachinohe)

structures under the 1940 Imperial Valley Earthquake (El Centro, N–S component, peak ground velocity (PGV) = 0.5 m/s) and the 1968 Tokachi-oki Earthquake (Hachinohe, N–S component, PGV = 0.5 m/s), respectively. Figs. 9 and 10 depict the corresponding response histories of the controlled structure equipped with RILD elements. It can be observed from Figs. 7-10 that compared with the proportional and distributed RILD elements having equal sum of coefficients, the optimally placed RILD elements are much more effective in reducing the inter-story drifts without compromising the floor response acceleration. This example verifies the effectiveness of the developed optimal RILD placement method for seismic vibration mitigation of a multi-story shear building model.

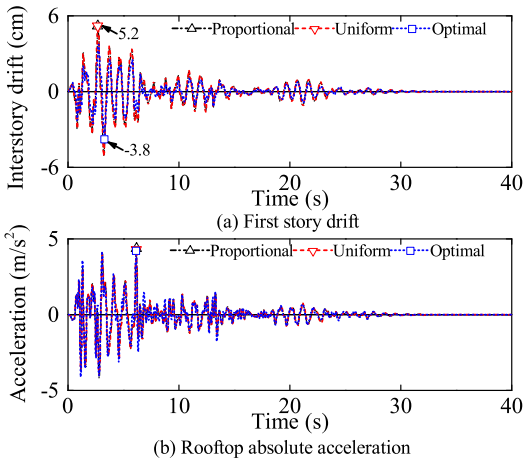

Figure 9: Structural Response histories (El Centro)

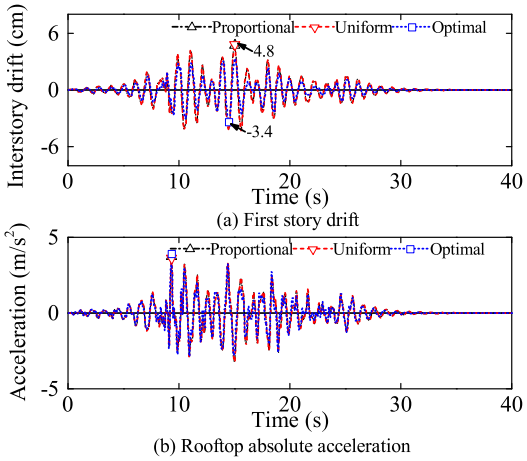

Figure 10: Structural Response histories (Hachinohe)

4.2. Parametric studies

Here, we further increase the sum of complex stiffness coefficients of RILD elements and investigate the distribution pattern variation of optimally designed RILD elements at different damping levels. To this end, the sum of the coefficients of proportionally designed RILD elements is considered, $w = \mathbf{1}\mathbf{k}_{\mathrm{d}} = \eta\mathbf{1}\mathbf{k}$, and the loss factor η is increased from 0 to 0.16 with an interval of 0.002. By applying the developed procedure, the optimally designed coefficients of RILD elements can be determined. Figs. 11 and 12 depict the corresponding objective functions and the designed coefficients of RILD elements at different damping levels. For comparison, the sums of the fundamental modal RAFs of the inter-story drift of the structure equipped with proportionally and uniformly distributed RILD elements are also plotted. It should be mentioned that the optimally designed coefficients of RILD elements at the other stories are zeros in this case studies, and thus they are not shown in Fig. 12 for brevity.

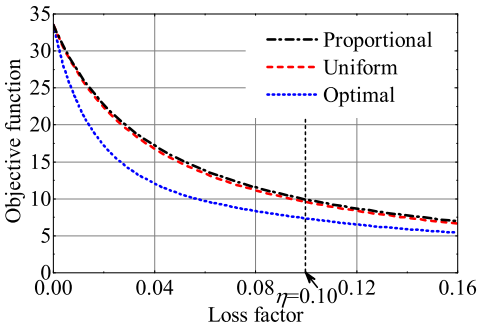

Figure 11: Objective functions

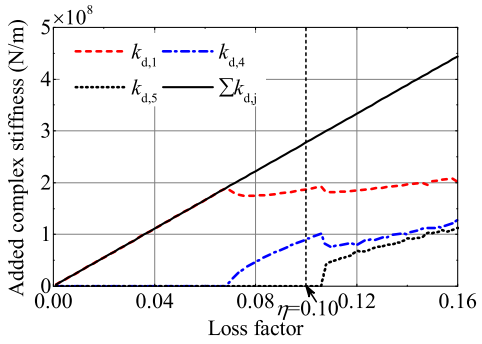

Figure 12: Optimally designed complex stiffness coefficients

It is observed from Fig. 11 that the objective functions decrease with the increase of the sum of complex stiffness coefficients of RILD elements (or loss factors), and the lowest objective functions among the three different cases at the same damping level are achieved by the optimally designed RILD elements. This further verifies the effectiveness of the developed optimal design method.

It is observed from Fig. 12 that with $\eta \in [0, 0.16]$, there exist three different patterns for the optimal distribution of RILD elements in the benchmark structure. At low damping levels, the RILD elements are installed at the first story only. Gradually, as the sum of RILD complex stiffness coefficients or loss factor increases, part elements start

to be distributed at the fourth story, and then they are distributed at the first, fourth, and fifth stories. This example verifies that the developed procedure can well adapt the distribution pattern variation of added RILD elements in a multi-story shearing building structure.

4.3. Comparison between different types of dampers

4.3.1. Performance curves

In order to further illustrate the benefit of RILD incorporated in multi-story shear buildings, the seismic responses of the benchmark building structure equipped with additional optimally placed LVD and RILD elements are compared.

To this end, the maximum value of the sum of peak damping forces of added damping elements used in the structure normalized by the total structural weight W, *i.e.*, $I_1 = \sum \max_t(|\mathbf{f}_d(t)|)/W$, is considered as a cost-related index in this study, because the damper force is directly related with the costs of a damper and its supporting members in engineering practice, and the maximum value of the peak inter-story drift angles of the controlled structure, *i.e.*, $I_2 = \max[\max_t(|\mathbf{u}(t)|./\mathbf{h})]$, where $\mathbf{h}$ denotes the structural height vector, is considered as a performance index. By increasing the sums of LVD and RILD coefficients and conducting structural response history analyses, we obtained the performance curves of the optimally designed LVD and RILD controlled structure in terms of the cost-related index I_1 and performance-related index I_2, respectively, as shown in Figs. 13 and 14. It should be noted that the developed procedure can be readily used for the optimal design of added LVD elements in the benchmark structure with slight modification.

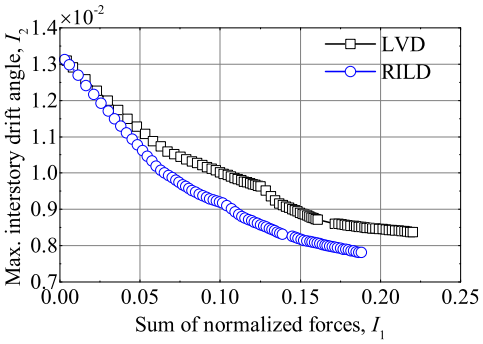

Figure 13: Performance curves (El Centro)

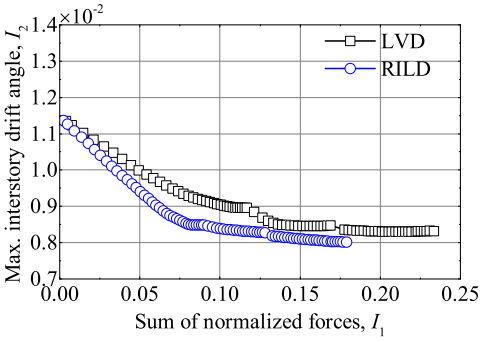

Figure 14: Performance curves (Hachinohe wave)

It is shown in Figs. 13 and 14 that with an equal cost-related index I_1, the RILD controlled structure generates smaller response inter-story drift than the LVD controlled structure. This verifies the benefit of RILD used for mitigating the seismic vibration of a multistory shear building structure subject to strong ground motions.

4.3.2. Comparison with equal cost-related indexes

To illustrate the performance difference of differently controlled structures, we assumed that the cost-related index is targeted at $I_1 = 0.15$ when the structure is subjected to the El Centro wave, and optimally determined the distribution of added LVD and RILD elements in the multistory building structure, respectively. The designed damper properties and the corresponding normalized control forces are listed in Table 3.

Fig. 15 plots the maximum floor responses of three types of structures subject to the El Centro wave. For example, Fig. 16 plots the floor response histories of those structures in terms of the second floor inter-story drift (which results in the largest inter-story drift angle) and rooftop response acceleration, when they are subjected to the El Centro wave. Fig. 17 plots the corresponding hysteresis loops of the added damping elements installed at the first and fourth stories.

It is shown in Figs. 15 and 16 that the RILD elements can be more effective than the LVD elements in reducing the structural inter-story drift and response absolute acceleration, when they are optimally designed with the equal cost-related indexes I_1 (i.e., sum of maximum normalized damping forces) for uses in a multistory building structure.

Table 3: Designed properties of LVD and RILD elements for comparison (El Centro wave)

j	LVD		RILD	
	$c_{d,j}$ (kN·s/m)	Normalized control force	$k_{d,j}$ (kN/m)	Normalized control force
1	57 411	0.114	182 420	0.091
4	22 604	0.036	79 806	0.033
5	0	0	54 300	0.026
other	0	0	0	0
sum	80 015	$I_1 = 0.15$	316 526	$I_1 = 0.15$

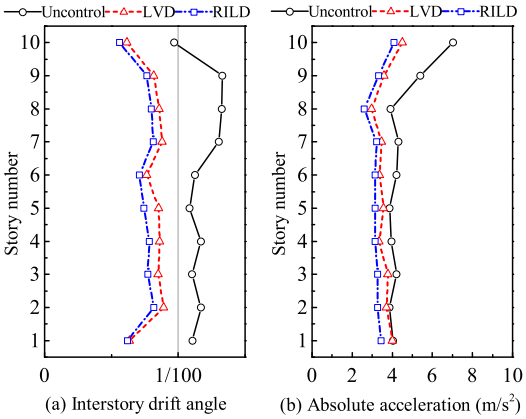

Figure 15: Maximum floor responses (El Centro)

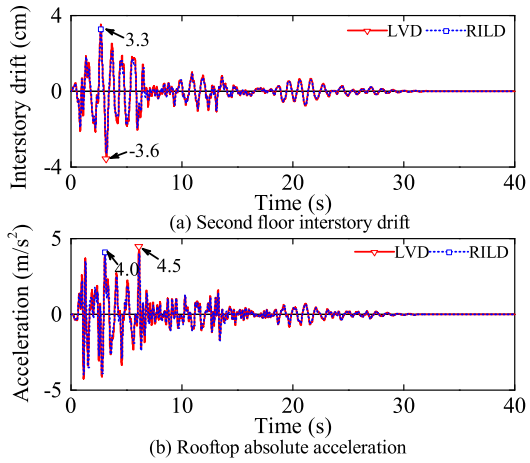

Figure 16: Structural response acceleration (El Centro)

Furthermore, a large number of response history analyses are conducted to investigate the performance of the RILD optimally-controlled structure under ground motions containing various phase properties. To this end, three types of recorded excitations are employed for time-history dynamic analyses. According to the design practice in Japan [37], the three natural records were scaled such that their peak ground velocities (PGVs) are equal to 0.5 m/s, which corresponds to design level earthquakes. Table 4 lists details of these ground motions. Each time-history excitation is identified by a number, as shown in Table 4.

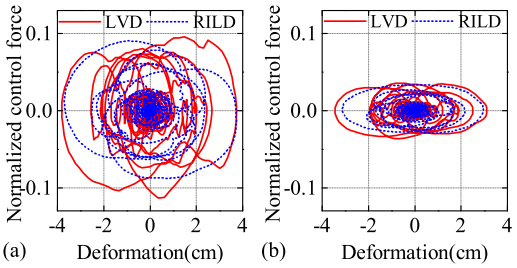

Figure 17: Hysteresis loops (El Centro): (a) first story, (b) fourth story

Table 4: Recorded ground motions

No.	Earthquake	Year	Station	Component	PGV
1	Imperial Valley	1940	El Centro	N-S	0.5
2	Kern County	1952	Taft	E-W	0.5
3	Tokachi-oki	1968	Hachinohe	N-S	0.5

Table 5 summaries the maximum seismic responses of the aforementioned LVD and RILD controlled structures under the chosen ground motions. It is shown that with equal cost-related indexes, the optimally designed RILD elements can be more effective than the viscous dampers in reducing the peak inter-story drift and floor response acceleration of a multi-story building structure under strong ground motions. This example also verifies that by minimizing the sum of structural inter-story drift RAFs, the developed method can be readily used to effectively mitigate the peak seismic vibration of a multi-story building structure under earthquake waves containing various phase properties.

Table 5: Maximum seismic responses of LVD and RILD controlled structures

No.	LVD			RILD		
	I_1	I_2	Floor acc.(m/s^2)	I_1	I_2	Floor acc.(m/s^2)
1	0.15	1/112	4.49	0.15	1/122	4.08
2	0.15	1/118	4.73	0.14	1/122	4.37
3	0.14	1/130	3.92	0.15	1/135	3.83
Max.	0.15	1/112	4.79	0.15	1/122	4.08

5. Conclusions

In this paper, we presented a gradient-based optimization method of placing RILD elements for seismic vibration mitigation of a multi-story building structure. Firstly, the relative displacement and absolute acceleration RAFs of the RILD controlled SDOF system were investigated by considering various damping levels. It is revealed that increasing RILD can effectively reduce the structural resonant responses without compromising the responses at high-frequency regions. This is one of the main advantages of RILD over the conventional LVD used for structural vibration mitigation.

A ten-story benchmark building structure was employed as an analytical example to verify the effectiveness of the proposed method. The conventional stiffness proportional and uniform distribution methods were considered for comparison with the proposed method. It was shown that with equal sum of RILD complex stiffness coefficients, the proposed method contributed to smaller structural vibration responses than the conventional methods.

Parametric studies were conducted to investigate the effect of RILD on the performance of the optimally controlled structure by gradually increasing the sum of complex stiffness efficients. The performance curves of the RILD controlled structure were obtained and compared with those of the controlled structure equipped with optimally placed viscous dampers. It is suggested that with equal sum of control forces, the optimally placed RILD elements can be more effective than viscous dampers in mitigating the inter-story drift and floor response acceleration of a multi-story building structure under strong ground motions containing various phase properties.

Acknowledgments

The authors gratefully acknowledge the support by the National Natural Science Foundation of China (No. 52208314 and No. 51838006), the National Key R&D program of China (No. 2023YFC3805700), and the China Postdoctoral Science Foundation (No. YJ20210457 and No. 2022M711258).

References

[1] R. Ma, K. Bi, H. Hao, Inerter-based structural vibration control: A state-of-the-art review, Engineering Structures 243 (2021) 112655.

[2] A. Rahgozar, H. E. Estekanchi, S. A. Mirfarhadi, On optimal triple friction pendulum base-isolation design for steel moment-frame buildings employing value-based seismic design methodology, Journal of Building Engineering 63 (2023) 105494.

[3] M. Ghandil, H. T. Riahi, F. Behnamfar, Numerical and experimental studies on a new metallic-yielding pistonic damper based on pure-bending flexural yielding mechanism, Journal of Building Engineering 78 (2023) 107690.

[4] Z. Zhang, K. Bi, H. Hao, P. Sheng, L. Feng, D. Xiao, Development of a novel deformation-amplified shape memory alloy-friction damper for mitigating seismic responses of rc frame buildings, Engineering Structures 216 (2020) 110751.

[5] D. De Domenico, G. Ricciardi, I. Takewaki, Design strategies of viscous dampers for seismic protection of building structures: a review, Soil dynamics and earthquake engineering 118 (2019) 144–165.

[6] O. Idels, O. Lavan, Optimization-based seismic design of steel moment-resisting frames with nonlinear viscous dampers, Structural Control and Health Monitoring 28 (1) (2021) e2655.

[7] M. A. Santos-Santiago, S. E. Ruiz, L. Cruz-Reyes, Optimal design of buildings under wind and earthquake, considering cumulative damage, Journal of Building Engineering 56 (2022) 104760.

[8] M. Yucel, G. Bekdaş, S. M. Nigdeli, S. Sevgen, Estimation of optimum tuned mass damper parameters via machine learning, Journal of Building Engineering 26 (2019) 100847.

[9] F. Yang, R. Sedaghati, E. Esmailzadeh, Vibration suppression of structures using tuned mass damper technology: A state-of-the-art review, Journal of Vibration and Control 28 (7-8) (2022) 812–836.

[10] T. Konar, A. Ghosh, A review on various configurations of the passive tuned liquid damper, Journal of Vibration and Control 29 (9-10) (2023) 1945–1980.

[11] Z. Zhao, R. Zhang, Y. Jiang, C. Pan, A tuned liquid inerter system for vibration control, International Journal of Mechanical Sciences 164 (2019) 105171.

[12] K. Ikago, K. Saito, N. Inoue, Seismic control of single-degree-of-freedom structure using tuned viscous mass damper, Earthquake Engineering & Structural Dynamics 41 (3) (2012) 453–474.

[13] H. Luo, R. Zhang, D. Weng, A hybrid control method to reduce the seismic response of a liquid storage tank, in: ASME Pressure Vessels and Piping Conference, Vol. 5, 2016, pp. PVP2016–63569.
[14] H. Luo, R. Zhang, D. Weng, Mitigation of liquid sloshing in storage tanks by using a hybrid control method, Soil Dynamics and Earthquake Engineering 90 (2016) 183–195.
[15] Z. Tang, H. Zhu, H. Luo, T. Li, Performance of a force-restricted viscous mass damper incorporated into base-isolated liquid storage tanks, Structures 61 (2024) 106002.
[16] H. Zhu, Z. Tang, H. Luo, S. Weng, A force-restricted inerter damper for enhancing the resilience of seismically isolated structures, Engineering Structures 313 (2024) 118268.
[17] A. A. Sarlis, D. T. R. Pasala, M. Constantinou, A. Reinhorn, S. Nagarajaiah, D. Taylor, Negative stiffness device for seismic protection of structures, Journal of Structural Engineering 139 (7) (2013) 1124–1133.
[18] H. Luo, C. Chong, K. Ikago, A. Keivan, B. Phillips, Passive implementation of rate-independent linear damping using a negative stiffness element, Proceedings of the 11th U.S. National Conference in Earthquake Engineering, Earthquake Engineering Research Institute, Los Angeles, CA, 2018.
[19] H. Zhu, Z. Tang, H. Luo, Feasibility analyses of negative-stiffness dampers for seismic performance enhancement of a base-isolated liquid storage tank, Soil Dynamics and Earthquake Engineering 164 (2023) 107575.
[20] H. Luo, H. Zhu, K. Ikago, Optimal design of negative-stiffness dampers for improved efficiency of structural seismic isolation, Journal of Building Engineering 68 (2023) 106172.
[21] Z. Zhao, X. Hu, Q. Chen, K. Yang, C. Liao, R. Zhang, Negative stiffness-enhanced seismic damping technology for an over-track complex with concrete-encased steel columns, Journal of Building Engineering 73 (2023) 106722.
[22] N. Myklestad, The concept of complex damping, Journal of Applied Mechanics (1952) 284–286.
[23] S. H. Crandall, The role of damping in vibration theory, Journal of sound and vibration 11 (1) (1970) 3–18.
[24] J. A. Inaudi, J. M. Kelly, Optimum damping in linear isolation systems, Earthquake engineering & structural dynamics 22 (7) (1993) 583–598.
[25] K. Ikago, N. Inoue, Behavior of rate-independent linear damping incorporated into long-period structures subjected to strong ground motions, Proceedings of the 6th World Conference on Structural Control and Monitoring, Barcelona, Spain, 2014, pp. 1116–1124.
[26] T. Caughey, Vibration of dynamic system with linear hysteretic damping (linear theory), Proceedings of 4th U.S. National Congress of Applied Mechanics, ASME, New York, 1962, pp. 87–97.
[27] H. Luo, K. Ikago, Unifying causal model of rate-independent linear damping for effectively reducing seismic response in low-frequency structures, Earthquake Engineering & Structural Dynamics 50 (9) (2021) 2355–2378.
[28] M. A. Biot, Linear thermodynamics and the mechanics of solids, Proceedings of the 3rd U.S. National Congress of Applied Mechanics, ASME, New York, 1958, pp. 1–18.
[29] N. Makris, Causal hysteretic element, Journal of engineering mechanics 123 (11) (1997) 1209–1214.
[30] N. Nakamura, Practical causal hysteretic damping, Earthquake Engineering and Structural Dynamics 36 (5) (2007) 597–617.
[31] G. Muravskii, Linear models with nearly frequency independent complex stiffness leading to causal behaviour in time domain, Earthquake engineering and structural dynamics 36 (1) (2007) 13–33.
[32] A. Reggio, M. De Angelis, Modelling and identification of structures with rate-independent linear damping, Meccanica 50 (3) (2015) 617–632.
[33] P. Deastra, D. Wagg, N. Sims, M. Akbar, Tuned inerter dampers with linear hysteretic damping, Earthquake Engineering & Structural Dynamics 49 (12) (2020) 1216–1235.
[34] Y. Tian, Y. Fei, Y. Huang, X. Lu, A universal rate-dependent damping model for arbitrary damping-frequency distribution, Engineering Structures 255 (2022) 113894.
[35] A. Keivan, B. M. Phillips, M. Ikenaga, K. Ikago, Causal realization of rate-independent linear damping for the protection of low-frequency structures, Journal of Engineering Mechanics 143 (9) (2017) 04017058.
[36] A. Keivan, B. M. Phillips, K. Ikago, Adaptive causal realization of rate-independent linear damping, Engineering Structures 167 (2018) 256–271.
[37] H. Luo, K. Ikago, C. Chong, A. Keivan, B. Phillips, Performance of low-frequency structures incorporated with rate-independent linear damping, Engineering Structures 181 (2019) 324–335.
[38] W. Liu, K. Ikago, Experimental study of earthquake input energy of low-frequency structures equipped with a passive rate-independent damping device, Structural Control and Health Monitoring 29 (2) (2022) e2883.
[39] W. Liu, K. Ikago, Performance of a passive rate-independent damping device in a seismically isolated multistory building, Structural Control and Health Monitoring 29 (6) (2022) e2941.
[40] H. Luo, Z. Tang, H. Zhu, A novel physical device to realize rate-independent linear damping for performance enhancement of seismically isolated structures, Engineering Structures 278 (2023) 115491.
[41] Z. Wu, W. Liu, K. Ikago, Feasibility study of a practical causal rate-independent damping device for the improved performance of seismic isolated structures, Engineering Structures 275 (2023) 115305.
[42] H. Zhu, Z. Tang, H. Luo, Seismic performance of a base-isolated flexible liquid storage tank equipped with a novel rate-independent damping device, Structures 51 (2023) 215–225.
[43] H. Luo, Z. Tang, H. Zhu, High-performance isolation systems with rate-independent linear damping for seismic protection of high-rise buildings, Soil Dynamics and Earthquake Engineering 171 (2023) 107976.
[44] R.-H. Zhang, T. Soong, Seismic design of viscoelastic dampers for structural applications, Journal of Structural Engineering 118 (5) (1992) 1375–1392.
[45] B. Wu, J.-P. Ou, T. Soong, Optimal placement of energy dissipation devices for three-dimensional structures, Engineering Structures 19 (2) (1997) 113–125.
[46] I. Takewaki, Optimal damper placement for minimum transfer functions, Earthquake Engineering & Structural Dynamics 26 (11) (1997) 1113–1124.
[47] I. Takewaki, S. Yoshitomi, K. Uetani, M. Tsuji, Non-

monotonic optimal damper placement via steepest direction search, Earthquake engineering & structural dynamics 28 (6) (1999) 655–670.

[48] J.-H. Park, J. Kim, K.-W. Min, Optimal design of added viscoelastic dampers and supporting braces, Earthquake engineering & structural dynamics 33 (4) (2004) 465–484.

[49] O. Lavan, R. Levy, Optimal design of supplemental viscous dampers for linear framed structures, Earthquake engineering & structural dynamics 35 (3) (2006) 337–356.

[50] Y. Kanno, Damper placement optimization in a shear building model with discrete design variables: a mixed-integer second-order cone programming approach, Earthquake engineering & structural dynamics 42 (11) (2013) 1657–1676.

[51] C. A. Martínez, O. Curadelli, M. E. Compagnoni, Optimal placement of nonlinear hysteretic dampers on planar structures under seismic excitation, Engineering Structures 65 (2014) 89–98.

[52] H. Shen, R. Zhang, D. Weng, C. Gao, H. Luo, C. Pan, Simple design method of structure with metallic yielding dampers based on elastic–plastic response reduction curve, Engineering Structures 150 (2017) 98–114.

[53] N. Pollini, O. Lavan, O. Amir, Minimum-cost optimization of nonlinear fluid viscous dampers and their supporting members for seismic retrofitting, Earthquake Engineering & Structural Dynamics 46 (12) (2017) 1941–1961.

[54] S. H. Sanati, A. Karamodin, Optimum seismic design of frame structures with and without metallic yielding dampers considering life-cycle cost, Journal of Building Engineering 76 (2023) 107335.

[55] L. Hao, M. Liu, J. Li, P. Tan, D. Wu, Multi-performance oriented seismic design of viscoelastic dampers for structural retrofitting, Journal of Building Engineering (2024) 108657.

[56] A. K. Chopra, Dynamics of structures: theory and applications to earthquake engineering, Vol. 2, Prentice Hall Englewood Cliffs, NJ, 1995.

[57] B. Lord Rayleigh, J W S, The Theory of Sound, Vol. 1, London, Macmillan and co., 1877.

[58] A. Kimball, D. Lovell, Internal friction in solids, Physical Review 30 (6) (1927) 948.

[59] K. Ikago, Y. Sugimura, K. Saito, N. Inoue, Modal response characteristics of a multiple-degree-of-freedom structure incorporated with tuned viscous mass dampers, Journal of Asian Architecture and Building Engineering 11 (2) (2012) 375–382.